N-type thermoelectric bulk composite based on poly(nickel-ethylenetetrathiolate): the positive effect of porosity on decreasing thermal conductivity

Swapneel Vijay Thakkar, Turkan Nabiyeva, Quentin Weinbach, Harsh Bhatia, Zilu Liu, Tom Ferté, Cédric Leuvrey, Alain Carvalho, Bob Schroeder, Laure Biniek

N-type thermoelectric bulk composite based on poly(nickel-ethylenetetrathiolate): the positive effect of porosity on decreasing thermal conductivity

Swapneel Vijay Thakkar [1], Turkan Nabiyeva [1], Quentin Weinbach [1], Harsh Bhatia [2], Zilu Liu [2], Tom Ferté [3], Cédric Leuvrey [3], Alain Carvalho [1], Bob C. Schroeder [2], Laure Biniek [1]*

1-Université de Strasbourg, CNRS, Institut Charles Sadron UPR22, F-67000 Strasbourg, France

2-Department of Chemistry, University College London, 20 Gordon Street, London WC1H 0AJ, United Kingdom

3- Institut de Physique et Chimie des Matériaux de Strasbourg, CNRS-Université de Strasbourg, UMR7504, Strasbourg, France

Contact: laure.biniek@ics-cnrs.unistra.fr

Abstract:

Recent progress in the research of *n*-type materials for organic thermoelectrics has drawn the attention to the metal coordination polymer poly(nickel-ethylenetetrathiolate) (poly(Ni-ett)). These polymers have excellent stability in air because their backbone structure is composed of air-stable ligands and exhibit good electronic properties when pressed into pellets or grown into crystals. However, due to their brittle nature and limited solubility, they are often blended with solution processable but electrically insulating polymers to produce composite films. Herein, we demonstrate the possibility of exploiting the 3D structuring ability of a polymer scaffolding matrix (based on polyvinylidene fluoride (PVDF)) to fabricate porous bulk structures. Porosity is introduced to reduce the lattice contribution to the thermal conductivity and used as a lever to increase the thermoelectric efficiency of the composite aerogel poly(Ni-ett): PVDF. For practical applications, these materials have great potential for vertical thermoelectric generators, as the low thermal conductivity and millimetre-thick samples would allow a thermal gradient to be maintained across it (without actively cooling one side, as in the case of certain thin-film technologies). In this manuscript, we present an original approach for the fabrication of novel *n*-type polymer aerogels resulting in lightweight and bulk size thermoelectric materials. The composite aerogels

exhibit a low thermal conductivity of 52 mW m^{-1} K^{-1}, and their figure of merit zT is comparable to the dense neat pellet with reasonable stability over six months.

1. Introduction:

Over two-thirds of the primary energy produced is discharged into the environment as waste heat, which, if recovered, could potentially be one of the largest secondary sources of clean energy [1]. Among the various sustainable waste heat recovery technologies available, thermoelectric generators (TEGs) are of great interest due to their ability to convert heat into electricity via the Seebeck effect [2]. The thermoelectric (TE) efficiency of materials is given by $zT = \sigma S^2 T/\kappa$ [where, σ is the electrical conductivity, S, the Seebeck coefficient, T the temperature, and κ the thermal conductivity]. In this context, conducting polymers (CPs) could convert low-grade heat (from various low-temperature (<150 °C) heat sources found in factories, vehicles [3] and even body heat [4]) into electricity due to their high electrical and low thermal conductivities. CPs offer good mechanical properties and can be produced on a large scale using low-cost manufacturing technique, giving them the potential to complement inorganic materials [5].

In the last decade, significant progress has been made with *p*-type CP such as doped poly(thiophene) derivatives (PEDOT:PSS, P3HT, PBTTT), which exhibit electrical conductivities greater than 100 S cm^{-1} [6-7]. Despite these promising properties, only a few examples of CPs based TEG have been produced, mainly due to the lack of stable and high performing *n*-type CP counterparts, which resulted in low power output when incorporated into a TEG [8-11]. In this context, metal-organic coordination polymers designed around a hybrid backbone using inorganic cations linked via organic ligands (such as poly(M-ett), where M = metal ion and ett = ethylenetetrathiolate) offer great potential. These materials exhibit good electrical conductivity and are known to be stable in air [11-14]. Sun et al. were the first to investigate the TE properties of these materials [15]. Poly(M-ett)s exhibit either *p*- or *n*-type behaviours depending on the nature and oxidative state of the metal centre. For example, poly(Cu-ett) demonstrates a positive *S* value, whereas poly(Ni-ett) shows a negative *S* value [15, 16]. Despite the promising TE properties exhibited by these intrinsic conducting materials, their complex synthesis and poorly understood reaction mechanism

result in significant variation of properties for the same material, posing significant challenges [11]. In addition, scaling up the synthesis of poly(M-ett) can be challenging due to inhomogeneities in the reaction mixture [17]. Despite these drawbacks, the outstanding electronic properties of metal-organic coordination polymers have motivated researchers to explore new possibilities to incorporate them into the next generation of thermoelectric energy harvesting devices (see Table 1).

Owing to their insolubility, poly(M-ett) are currently studied in the form of either dense pellets or composite films (blended with a binder polymer) [11]. The insoluble poly(M-ett) can be dispersed in an organic polymer matrix such as polyvinylidene fluoride (PVDF) or poly(methylmethacrylate) (PMMA) using ball milling. However, the insulating nature of the matrices negatively impacts the TE properties of composite films compared to the neat poly(M-ett) [18]. For instance, Jiao et al. produced poly(Ni-ett) pellets exhibiting a power factor ($PF = \sigma S^2$) of 3.7 μW $m^{-1}K^{-2}$. When processed as thin films with PVDF, the power factor drastically decreased to 0.4 μW $m^{-1}K^{-2}$ [16], (see Table 1). Researchers have made efforts to increase the power factor by adding carbon nanotubes (CNT) to such blends to increase the number of charge carriers in the system [19]. Although these ternary blends recorded an increase in electrical conductivity by a factor of two, they no longer exhibited *n*-type behaviour.

An alternate approach to improve the TE efficiency of poly(Ni-ett) based composites is to decrease their thermal conductivity (κ), instead of focussing on enhancing their electronic properties. For electrically conductive materials, κ is composed of two components, namely $\kappa_{lattice}$ and $\kappa_{electronic}$. The $\kappa_{electronic}$ component is dependent on the electrical conductivity of the material (based on the Wiedemann–Franz law). Therefore, it cannot be used to modulate the overall thermal conductivity [20]. While $\kappa_{lattice}$ component is dependent on the material microstructure (such as density, morphology, etc), which can be tuned to reduce the thermal conductivity. In this regard, introducing pores into the material with pore sizes similar to or smaller than the mean free path of air molecules (≈ 70 nm) is likely to reduce the gaseous component of $\kappa_{lattice}$ (known as Knudsen effect) [21]. Whereas, increasing the porosity of the material (i.e. reducing its density) should decrease the solid component of $\kappa_{lattice}$ [22]. Hence, designing a highly porous material with small pore sizes (< 70 nm) has the potential to decrease the overall κ. In such a case, fabricating poly(M-ett) composites in the form of an

aerogel (a three-dimensional bulk solid with low density and abundant mesopores) is expected to substantially boost the thermal resistance, thus enhancing the TE properties.

Processing conducting polymers into bulk aerogels is of great interest in the field of organic thermoelectricity as it provides technological benefits such as (i) maintaining the thermal gradient within the material, due to the ultra-low κ, and (ii) producing out-of-plane TEGs. The research into thermoelectric aerogels is still nascent and there are only few studies that demonstrate their potential on *p*-type materials [23–28]. To the best of our knowledge, all the reports on *n*-type aerogels are based on CNTs, which are functionalized to change from *p*-type to *n*-type. However, due to stability issues in air, they revert to their original *p*-type behaviour [29-31]. Thus, the production of aerogels utilising poly(Ni-ett) would open up a new avenue towards creating air-stable *n*-type materials featuring promising thermoelectric properties.

Table 1: *TE properties of Ni-ett and its processed materials reported in the literature.*

Material	**Form**	**σ** **(S cm^{-1})**	**S** **(μV K^{-1})**	**κ** **(W m^{-1}K^{-1})**	**PF** **(μW m^{-1}K^{-2})**	**zT** **(calculated)**	**Reference**
Na[Ni-ett]	Pellet	40	-75	0.16-0.28	23	0.1-0.2 (at 400 K)	[15]
K [Ni-ett]	Pellet	44	-122	0.17-0.31	66	0.1-0.2 (at 400 K)	[15]
K [Ni-ett]	Film Ni-ett: PVDF (2:1 ratio) annealed at 160°C film (2-5μm thick)	8 2	-67 -45	- -	3.7 0.43	- -	[16]
Na [Ni-ett]	Pellet Ni-ett: PVC (10:3 ratio)	9×10^{3} 4.4×10^{-3}	-42 -35	- -	1.6×10^{-3} 4.9×10^{-4}	- -	[32]
K_x [Ni-ett]	Pellet	24.3	-33.9	-	2.79	-	[33]
Ni-ett	potentiostatic deposition at 0.6 V	67.5	-139	0.28	131.6	0.08 (at 300 K)	[34]
K [Ni-ett]	Ni-ett: PVDF (4:1 ratio) film (2-5μm thick); 24h air	5	-27	-	0.38		[17]

	exposure during synthesis Ni-ett: PVDF (4:1 ratio) film (2-5µm thick); 30 min air exposure during synthesis	 43	 -33	 -	 4.7		
Na [Ni-ett]	Ni-ett: PVDF (4:1 ratio) annealed at 160°C film (5-10 µm thick)	23	-74	-	13	-	[18]
Li [Ni-ett]	Ni-ett: PVDF (4:1 ratio) annealed at 160°C film (5-10 µm thick)	37	-50	-	9	-	[18]
K [Ni-ett]	Ni-ett: PVDF (4:1 ratio) annealed at 160°C film (5-10 µm thick)	2	-99	-	2	-	[18]
Na [Ni-ett]	Ni-ett: PVDF (4:1 ratio) as cast film Annealed film at 160°C (5-10 µm thick)	6 23	-28 -74	- -	0.5 12.5	- -	[35]
Ni-ett	Block Ni-ett:PVC (10:3 ratio) film Ni-ett:CNT:PVC (10:8:3 ratio) film	3.6×10^{-2} 4.4×10^{-3} 429	-39 -32.9 30	- - 0.07	5.7×10^{-3} 4.7×10^{-4} 39	- - 0.2 (at 340 K)	[19]

In this manuscript, we present a novel work on the preparation of *n*-type composites aerogels based on poly(Ni-ett) and PVDF for TE applications. PVDF aerogels appear as the scaffolding matrix of choice for both, *i*) its good compatibility with poly(Ni-ett) and *ii*) its low

thermal conductivity [36]. Herein, we designed a methodology to well-dispersed poly(Ni-ett) within the scaffold during the PVDF gelation. Furthermore, we were able to maintain the unique mesoporous structure of the gel after drying under supercritical conditions. The electronic and thermal properties of the composite aerogels were characterized using the methodology developed from our previous study [25]. Overall, we successfully developed a sound methodology to fabricate millimetre thick *n*-type composites aerogels via a multistep synthetic process, and highlighted their potential for integration into the next generation of vertical thermoelectric generators.

2. Experimental Section:

2.1 Materials:

All chemicals for the aerogel synthesis were commercially available and purchased from the following suppliers: *N,N*-dimethylacetamide (DMAc, > 99% Sigma- Aldrich), de-ionized water, polyvinylidene fluoride (PVDF, M_w > 500 000 g mol^{-1} eq. PS, PDI > 1.7, Polysciences), absolute ethanol (EtOH, anhydrous, Roth), silver paste from Agar Scientific (AGG3691), liquid CO_2 (Air Liquide), liquid N_2 (Air Liquide).

2.2 Methods:

Poly(nickel-ethylenetetrathiolate) synthesis

Poly(Ni-ett) materials were synthesized following a published report [37]. As a reference sample, poly(Ni-ett) powder was pressed into free-standing pellets using a hydraulic press (3 Ton/13 mm^2, pellet thickness = 0.4 mm, density = 1.55 g cm^{-3}). The characterizations of the reference poly(Ni-ett) pellets should be taken with caution, as their properties are dependent on the pellet density, especially when compared to the literature.

PVDF gels and aerogels

The PVDF gels were prepared by the phase inversion method (with the use of DMAc as solvent and water as non-solvent). The gelation conditions of the matrix material (i.e. PVDF) was standardized by considering the dispersion conditions of poly(Ni-ett) in DMAc. Briefly, a

mixture of water/ DMAc (1:9 v/v) and PVDF (10 wt%) was heated at 90°C to dissolve the polymer. The solution was then left to cool down at ambient temperature ($PVDF_{amb}$) or quenched into liquid nitrogen ($PVDF_{N2L}$) to form wet gels. After solvent exchange of the wet gels with ethanol, the alcogels were dried by supercritical CO_2 drying (see the conditions of drying below) to obtain the PVDF aerogels. The PVDF aerogels have a density of 0.13 - 0.16 g cm^{-3} with almost no shrinkage after drying, which highlights that supercritical drying preserved the gel network.

Fabrication of PVDF:poly(Ni-ett) composite gels

The fabrication of the composites gels and aerogels are described in schematic SI1.

Composites gels of mass ratio between the poly(Ni-ett) and PVDF (2:1) were prepared by a multi-step process as shown in Figure 1. Step 1, 90 mg of the poly(Ni-ett) was milled with 0.9 mL of DMAc and 0.1 mL of water using agate cylindrical tube with a single agate ball (2 mm diameter). The milling was set 20 minutes (with an interval of 2 minutes after first 10 minutes) to obtain a homogenous dispersion. Step 2, the dispersion was then transferred to a stainless-steel mould (18 mm internal diameter, 20 mm depth, customized to open/close on either ends) and placed on a hot plate set at 95°C under stirring. Step 3, once the dispersion reached the set temperature (~20 minutes), 45 mg of PVDF was swiftly added into the mixture. Step 4, after PVDF was dissolved, the mould was removed from the heating plate and immersed quickly into liquid N_2 for 10 minutes to solidify the mixture. Step 5, the bottom end of the mould was dismantled and the frozen solid was immediately dropped into a 50 mL vial containing non-solvent (i.e. EtOH). This process led to an immediate formation of gel due to phase-inversion of the matrix. The gels were washed three times with EtOH, which was achieved by immersing the gels in EtOH and replacing fresh EtOH every 12 hours (gel image in Figure ESI2, supporting information). This step ensures the presence of EtOH in the pores of the composite gel which facilitates its supercritical drying with liquid CO_2.

Supercritical drying of gels:

The gels were dried based on the conditions set from our previous report [25]. Briefly, the hybrid gels were washed thoroughly after synthesis (with EtOH), and then loaded into an autoclave (manufactured by SFT-110 supercritical fluid extractor). 1mL of EtOH was added

onto the gels to prevent them from drying, and the autoclave was sealed. The liquid CO_2 tank was opened and the autoclave was filled with CO_2. To ensure that the state of CO_2 in the autoclave is liquid; the temperature was maintained below 20 °C and the pressure in the autoclave was increased from 750 to 1200 psi. The gel was soaked in pressurized liquid CO_2, during which the diffusion of solvents within the gels takes place. The mixture (liquid CO_2 + EtOH) was flushed by depressurizing the autoclave, and fresh liquid CO_2 was added by repressuring. This process was repeated for 5 times to ensure complete removal of EtOH from the gel. Next, the autoclave at 1200 psi was heated at 45 °C for 2 h, during which transition of CO_2 from liquid to supercritical phase takes place. The outlet valve was slightly opened to create a dynamic flow of supercritical CO_2 in the autoclave. The gel was kept under these conditions (45 °C and 1200 psi) for 1 h, following which the CO_2 tank was closed. The autoclave was vented by a slow release of pressure while keeping the temperature constant. After venting of supercritical CO_2 from autoclave was complete (approx. 30 min), the obtained aerogel was transferred to a vial. The vial was degassed for few minutes and then switched to argon atmosphere for storage. The aerogels have a density of ~ 0.34 g cm^{-3}, which was calculated based on the weight and the physical dimensions of the samples.

The porosity was estimated by the method reported by Wang and co-workers [38] by comparing the weight of aerogels before and after absorption of *n*-octanol. The aerogels were immersed into *n*-octanol for 2h. The surface was then blotted on filter paper and the samples weighed. The porosity was calculated using the following equation:

$$P = \frac{(m_o/\rho_o)}{(m_o/\rho_o) + (m_p/\rho_p)} \times 100\%$$

Where *P* is the porosity of the aerogel, m_p, the mass of the polymer aerogel, m_o, the mass of the absorbed *n*-octanol, ρ_p, the density of the polymer (ρ_{PVDF} = 1.78 g cm^{-3}), ρ_o, the density of *n*-octanol (0.83 g cm^{-3}).

2.3 Characterization methods:

(i) Physico-chemical characterizations:

Fourier transform infrared (FTIR) spectra were recorded on a Brucker vertex 70 in transmission mode, between 600 and 4000 cm^{-1} with a resolution of 2 cm^{-1} and an accumulation of 24 scans.

The textural properties of the prepared samples were studied by N_2 adsorption-desorption measurements at -196 °C (ASAP 2420 Micromeritics). The materials were degassed under vacuum at low temperature (40 °C) for 12 h to desorb the moisture before analysis. Specific surface area was calculated by Brunauer-Emmet-Teller (BET) method. Pore volume and pore distribution were determined using desorption branch by the Barrett-Joyner-Halenda (BJH) method.

Thermogravimetric analysis (TGA) was performed by using a Mettler Toledo device at a heating rate of 5 °C min^{-1} from room temperature to 800 °C under nitrogen atmosphere (50 mL min^{-1}).

Differential scanning calorimetry: melting and crystallization temperatures of the aerogels were determined by means of a DSC 8500 from PerkinElmer. Heating and cooling rates of 10 °C min^{-1} were used within a temperature range from 20 °C to 220 °C. The degree of crystallinity χ_c was evaluated by: $\chi_c = \Delta H_f/\Delta H_f^\circ$ with $\Delta H_f^\circ = 104.7$ J g^{-1} [39], the melting enthalpy for a 100 % crystalline sample of PVDF. The values are reported in Table SI1.

Wide angle X-ray scattering measurements (WAXS) were performed at the DiffériX platform of the Institut Charles Sadron on a Rigaku diffractometer. A monochromatic beam was obtained by projecting the primary beam from an X-ray generator (MicromaxTM-007 HF, operating power 40 kV - 30 mA, Cu-K radiation, wavelength 0.154 nm) onto a confocal mirror with a multilayer coating (Confocal MaxFluxTM Optic, Rigaku). After pinhole collimation, the size of the beam at the sample position was about 300 m. The scattered intensity was collected on Fuji imaging plates 10 cm downstream of the sample (transmission mode), covering a scattering angles range from 2=10 to 45°.

Scanning Electron Microscopy: Cross-sections of PVDF and composite aerogels were prepared using a razor blade. The samples were observed at 1 kV with a FEG-SEM Hitachi SU8010. The images were collected with the SE-in Lens detector.

Backscattering electrons images were obtained using the “in-chamber” dedicated backscattered electron detector of a Zeiss GeminiSEM 500 microscope at 8 kV.

(ii) Thermoelectric characterizations:

After the synthesis, the aerogels were first studied to evaluate the thermal conductivity, followed by electrical conductivity and Seebeck coefficient. To set the conditions for measurements and method of sample preparation, we followed a well-developed methodology from our earlier works on *p*-type aerogels [25, 40].

(a) The thermal conductivity of the aerogels was measured using the transient plane source (TPS) technique by utilizing a commercial Hot Disk (Hot Disk®, TPS 1000) apparatus. Here, the sensor of the instrument (radius 3.189 mm) was sandwiched between two identical aerogels, the setup was then placed under a metallic bell to avoid any interference with ambient air currents. The experiments were performed at ambient conditions (24°C), the input power and time duration were set at 7 mW and 40 s. The parameters met the best measurement conditions to be within the limits of total characteristic time (between 0.33 and 1), temperature increase and penetration depth of the aerogel sample [41]. The measurements were repeated five times with a time interval of 30 minutes between each trial.

For electronic properties, a Keithley 2634B source meter and a Lab Assistant Semi probe station were used to measure electrical conductivity and Seebeck coefficient of all samples. The measurements were conducted inside a Jacomex glovebox under N_2 atmosphere (≈ 1ppm O_2, ≈ 1ppm H_2O).

(b) To measure the electrical conductivity, the aerogels and the poly(Ni-ett) pellets were first degassed overnight at ultra-high vacuum (10^{-8} bar). Then, electrical resistance was measured on the samples using a standard collinear four probes method (probe space of 1.6 mm). The electrical resistivity and conductivity were then calculated using Haldor Topsøe geometrical factor [42].

(c) To measure Seebeck coefficient (S), the aerogels/ poly(Ni-ett) pellets were first attached to a copper plate. This was done by fixing the ends of its surface to a copper plate using a silver paste, which allows a good thermal contact between the sample and the plate (see

schematic Figure SI7, supporting information). The samples were then placed on a homemade setup made of two Peltier elements (one heating and the other cooling), separated by a 3 mm gap, that allows an in-plane controllable temperature gradient. Measurements were based on differential temperature method, during which the temperature difference between the two Peltier cells was increased gradually up to 12.8 K (starting from 293K) [43]. The voltage was measured directly on the silver paste that was in contact with the sample and the copper plate. For each set of temperature difference, the voltage was recorded for five trails with 20 s of time interval after each measurement. The Seebeck coefficient was calculated from the slope of voltage versus temperature difference curve. A typical curve in shown in Figure SI7 in supporting information.

3. Result and Discussion:

3.1 PVDF aerogels and PVDF:poly(Ni-ett) composite gels and aerogels

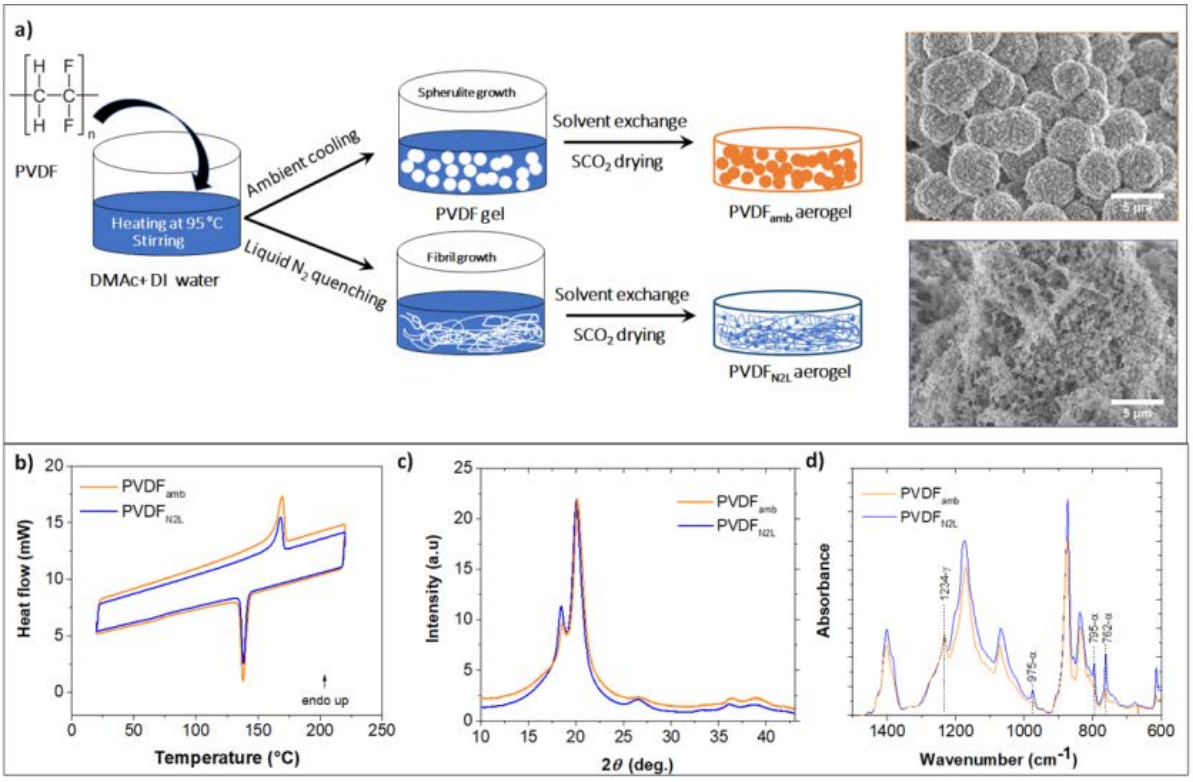

Figure 1: a) Schematic of PVDF gel synthesis *via* ambient cooling ($PVDF_{AMB}$, top) and rapid cooling ($PVDF_{N2L}$, bottom) and their corresponding SEM images. b-d) DSC, WAXS intensity profiles as a function of 2ϑ and IR spectrum of both PVDF aerogels, respectively.

The PVDF gelation conditions were first investigated using phase-inversion method prior to preparing the composite aerogels. Phase-inversion method is a technique widely used for preparation of porous thin films, where a surface coated with polymer solution is immersed in a non-solvent bath [44, 45]. However, when this method is exploited to prepare mm-thick gels; the non-solvent interacts non-uniformly with the polymer suspension. This leads to the formation of gels with an inhomogeneous microstructure throughout the gel with presence of macrovoids [45, 46]. In this work, the non-solvent (i.e., water) was directly mixed with solvent (i.e., DMAc) prior to dissolution of PVDF at 90°C, (rather than adding the non-solvent after the PVDF was dissolved) [46]. Upon cooling of the suspension to ambient temperature; liquid-liquid demixing takes place uniformly throughout the sample. This promotes nucleation and growth of PVDF spherulites interacting with each other and resulting in gel formation [47]. After solvent exchange with ethanol and drying with CO_2 in supercritical conditions, a white porous bulk solid was obtained (91 % porosity). Figure 1A displays the schematic of synthesis, and the resulting microstructure of the $PVDF_{amb}$ aerogel. PVDF spherulites of diameter ~ 5 μm act as individual building blocks, which are homogeneous and connected with each other (with tie chains) to form porous solid. The sample obtained by ambient cooling is semi-crystalline with a degree of crystallinity of 0.47 (see supporting information Table SI1 and DSC in Figure 1B). WAXS and IR spectroscopy of the $PVDF_{amb}$ aerogel are presented in Figure 1.C and D, respectively. The WAXS intensity profile shows a strong peak at 20.15° and medium peaks at 18.54° and 38.96°, which can be attributed to 110/101, 020 and 211 of monoclinic γ-phase crystal, respectively [47]. While, the IR peak at 1234 cm^{-1} is characteristic of the γ-phase [48]. These characterizations reveal that the crystalline structure of $PVDF_{amb}$ mainly consists of γ-phase (co-existing with α-phase). Despite their high porosity, the $PVDF_{amb}$ aerogels were brittle in nature. Additionally, the ambient cooling process is likely to lead to poly(Ni-ett) particle sedimentation (see Figure SI1b, supporting information) during the extended gelation process via liquid-liquid demixing of the suspension, posing another disadvantage. To overcome these issues, the gelation rate was increased by raising the cooling rate. This was achieved by quenching PVDF solutions into liquid Nitrogen (N_{2L}) to prepare gels, prior to solvent exchange and further drying under supercritical condition, providing $PVDF_{N2L}$ aerogels. Although the porosity of these samples (93 %) was similar to the $PVDF_{amb}$ aerogels, the SEM micrographs revealed a distinct

structure. Here, rapid cooling of the solution limited the nucleation of PVDF spherulites due to incomplete liquid-liquid demixing; thereby promoting a fiber like structure [47], which entangled with each other and with small spherulites (< 100 nm in diameter) (Figure 1A). The IR spectrum of $PVDF_{N2L}$ (Figure 1D) exhibits pronounced peaks at 975, 795 and 762 cm^{-1}, related to the α-phase [48]. While, WAXS data (Figure 1C) show peaks at 18.4 and 26.5°, which are more intense than for $PVDF_{amb}$, and which can be attributed to the 020 and 021 reflections of the monoclinic α-phase [48]. Therefore, the fiber-like structure can be attributed to the increase content of the α-phase of PVDF (co-existing with the γ-phase).

The increased cooling rate impacted the microstructure of the PVDF aerogels but not their degree of crystallinity or porosity which are requisite for reaching low thermal conductivity values. Interestingly, $PVDF_{N2L}$ and $PVDF_{amb}$ samples display similar thermal conductivity values in the range of 33-36 mW m^{-1} K^{-1}. This indicates that the dominant fibrillar α-phase samples formed during quenching did not significantly impact the thermal properties of the aerogels. The low thermal conductivity values are attributed to the mesoporous structure of the aerogels (see below).

In conclusion, the gelation process at high cooling rate (quenching in liquid nitrogen) was preferred to prepare the composite aerogels, as it prevents sedimentation of poly(Ni-ett) particles and a possible concentration gradient within the sample. In order to preserve the electronic properties of the poly(Ni-ett) as much as possible (and limiting the large scale phase separation of the two polymers), we opted for a loading ratio of 2:1 (by mass) of poly(Ni-ett) and PVDF, respectively. In the synthesis, the direct addition of poly(Ni-ett) during mechanical stirring of solvents was avoided - as they tend to agglomerate while mixing. Hence, ball-milling of poly(Ni-ett) particles with the solvents was utilized to grind the particles and obtain a more stable dispersion. The dispersion was then mixed with PVDF and the protocol of $PVDF_{N2L}$ was followed. The fabrication of the composite gels and aerogels is presented in the experimental part and on Figure 2.

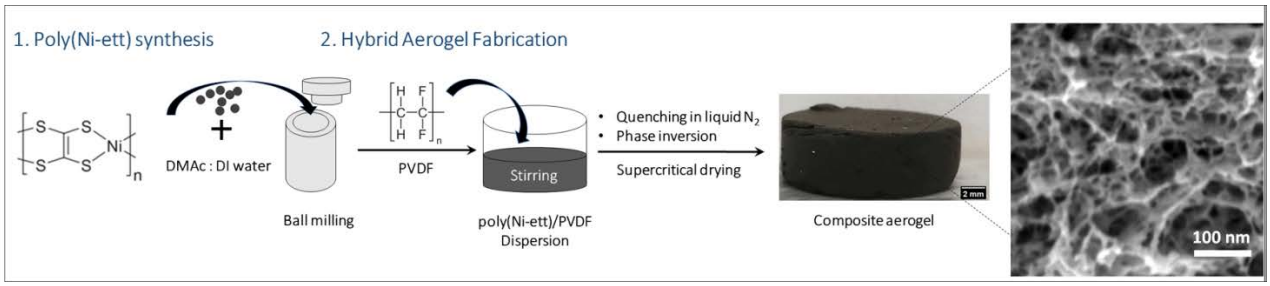

Figure 2: Schematic of the composite PVDF:poly(Ni-ett) aerogel fabrication and SEM image of its inner mesoporous and fibrillar structure.

The process yielded black and lightweight composite aerogels (density of ~ 0.34 g cm^{-3}). The crystalline degree of PVDF within the composite aerogels (0.40, see Figure SI3 and Table SI1 in supporting information) is slightly lower than for the neat PVDF aerogels (0.47). The crystalline phases, determined by IR (see Figure SI6, supporting information) is given as co-existence of both *γ* and *β*-phases (with new peaks originated at 1430 and 1274 cm^{-1}). This indicates that the addition of the poly(Ni-ett) impacts the PVDF chain conformation. Furthermore, the presence of β-phases in the PVDF matrix yield the potential to exploit its ferroelectric properties to enhance the thermoelectric properties further [49-51] In terms of thermal stability, as seen from the TGA data (supporting information, Figure SI5), the composite aerogels are stable up to 150°C (contact moisture is mostly desorbing at this temperature), which is higher in temperature when compared to the neat poly(Ni-ett).

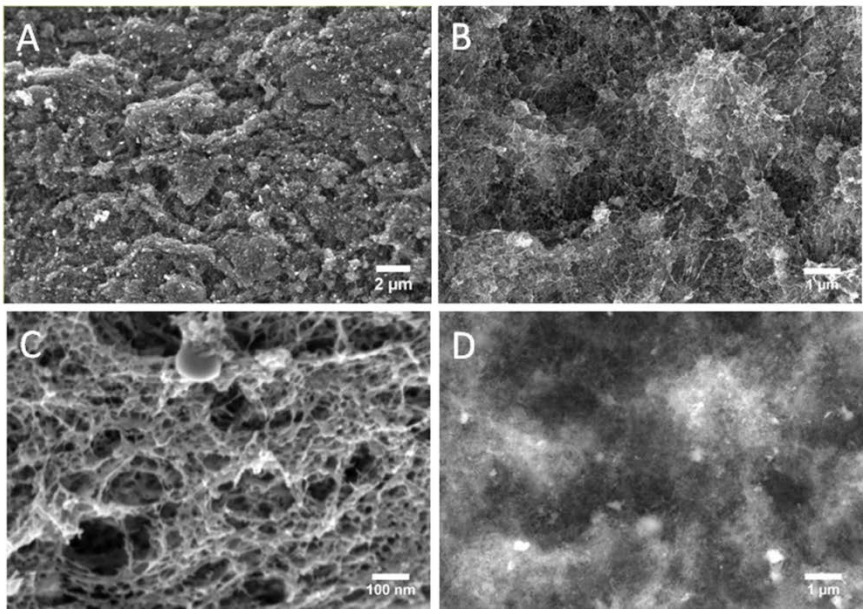

Figure 3: A-C: SEM images of the composite aerogels showing mesoporous structure with fibrillar network. D: Composition contrast BSE image (same area as B) showing poly(Ni-ett) particles (bright spots) embedded in the PVDF matrix.

SEM images of the composite aerogel at different magnifications are presented in Figure 3. The composite aerogel exhibited a mesoporous network with open cell pores (< 50 nm void size), which was formed due to polymer fibers interconnection at nanoscales (fibers thickness ~5-10 nm, see Figure 3 B-C). The textural properties were also confirmed by N_2 adsorption-desorption measurements. The shape of the isotherms (type IV, see Figure SI4, supporting information) shows the mesoporous nature of the samples. The BET specific surface area of the composite aerogel (84 $m^2\ g^{-1}$) is lower than that of the $PVDF_{N2L}$ aerogel (167 $m^2\ g^{-1}$), consistent with a lower pore volume with poly(Ni-ett) (0.43 and 0.74 $cm^3\ g^{-1}$, for the composite and the neat PVDF, respectively). In both samples, the specific surface areas are attributed to the mesopores of similar size (17 nm and 21 nm, for the composite and the $PVDF_{N2L}$ aerogels, respectively). From the t-plot treatment, it can be concluded that there are no micropores present in either samples.

This unique microstructure can be credited to the synthesis conditions, where; the liquid-liquid demixing process of the suspension was hindered due to the rapid freezing conditions and the presence of high amounts of poly(Ni-ett) in the mixture.

The dispersion of poly(Ni-ett) in the aerogel (Figure 3B) was investigated by measuring the backscattered electrons from the sample (Figure 3D). The bright regions in the micrograph are attributed to the poly(Ni-ett) sites due to their high atomic density, and indicates that the coordination polymer was homogeneously dispersed throughout the sample (bulk and surface). The average size of the particles was less than 100 nm with some of the largest cluster of particles being ~ 400 nm (Figure 3D). These agglomerated particles may be the cause of the lower pore volume and specific surface area compared to the neat PVDF aerogel.

3.2 Thermoelectric properties of the composite aerogels

Table 2: *Thermoelectric properties of the poly(Ni-ett) pellets vs the PVDF: poly(Ni-ett) composite aerogel. Errors represent the standard deviations of three to four measurements on one or two samples.*

Materials	**Conditions**	**Time**	**σ (S cm^{-1})**	**S (μV K^{-1})**	**PF (μW m^{-1}K^{-2})**	**κ (W m^{-1} K^{-1})**	**Calculated zT (at 300 K)**
Poly(Ni-ett) pellet	After Synthesis	0 days	12.5 ± 1.5	-26 ± 1	0.845	0.178 ± 0.009	1.4×10^{-3}
Composite aerogel (5 mm thick)	After synthesis	0 days	0.28 ± 0.02	-59 ±2	0.097	0.052 ± 0.005	5.6×10^{-4}
	Stored in air	6 months	0.015 ± 0.03	-89 ± 4	0.011	0.052 ±0.005	6.8×10^{-5}
	Stored in glove box	6 months	0.24 ± 0.02	-52 ± 2	0.065	0.053 ± 0.005	3.7×10^{-4}

The TE properties of the composite aerogels are presented in Table 1.

The composite poly(Ni-ett):PVDF aerogel showed an electrical conductivity of 0.28 S cm^{-1} and a negative Seebeck coefficient of -58.6 μV K^{-1}, confirming its n-type character. For comparison, the neat poly(Ni-ett) was also characterized as a pressed pellet; it showed a conductivity of 12.5 S cm^{-1} and a Seebeck coefficient of -26 μV K^{-1}. The lower charge conductivity value for the composite aerogels was expected, due to the presence of high air content within its structure (high porosity) and the influence of electrically insulating PVDF matrix, which prevents efficient and interconnected charge transport pathways. Based on our previous report on PEDOT:PSS aerogels [25], we expected the porosity to have little effect on the Seebeck coefficient. We attribute the observed increase in Seebeck coefficient for the composite aerogel (as compared to the dense neat pellet) to reduced percolation pathways in the composite aerogels, thereby hampering charge transport across the aerogels compared to the neat poly(Ni-ett) compressed pellets. The composite materials exhibit a power factor of 0.097 μW m^{-1}K^{-2}, which is an order of magnitude lower than that of the neat poly(Ni-ett). A similar behaviour was also observed for the power factor of composite thin films (poly(M-ett) blended with electrically insulating polymer), which have an order lower when compared to the neat poly(M-ett) counterpart (see Table 1) [16, 19, 32, 52].

Whilst PVDF improves the processability of the poly(Ni-ett) to prepare flexible films or porous solids, the blending hinders the charge transport properties of the composite. However, more interestingly, the effect of compositing and porous structure favours in

decreasing the thermal transport properties. It can be seen from Table 2, that the average thermal conductivity for composite aerogels was measured to be 0.052 W m^{-1} K^{-1}, which is three to four times lower than dense poly(Ni-ett) pellet (κ = 0.178 W $m^{-1}K^{-1}$). The thermal conductivity of composite aerogels is higher by a small margin when compared with the pure PVDF aerogels (κ = 0.033 – 0.036 W $m^{-1}K^{-1}$). This increase can be attributed to the slightly increased bulk density and the electronic contribution ($\kappa_{electronic}$) in the thermal conductivity of poly(Ni-ett). Most importantly, the decrease in the thermal conductivity of the composite aerogel compensates the decrease in electronic properties. Ultimately, the zT (at 300 K) of the composite aerogels at a loading ratio of 2:1 (poly(Ni-ett): PVDF) was calculated to be 5.6 × 10^{-4}, while the pressed poly(Ni-ett) pellets showed a value of 1.4 × 10^{-3}.

To test the stability of the composite aerogels in different atmospheres, half of the samples were stored under ambient conditions (room temperature, 20 °C and 40 % ambient humidity) and half under an inert atmosphere in a glove box. Their properties were measured after 6 months, as shown in Table 1. The electrical conductivity of the composite aerogel stored in air decreased over time (by more than an order of magnitude), while, the sample stored in the glove box did not show any significant decrease in values. The aerogel stored in the glove box showed no significant changes in Seebeck values, while the aerogel stored in ambient conditions showed a higher value (consistent with the decrease in electrical conductivity and possibly oxidation). The thermal conductivity (mainly related to a lattice contribution) was hardly affected over time (due to the stability of the porous structure). Overall, the stability of the composite aerogels prepared with poly(Ni-ett) was promising when compared with other *n*-type polymers.

The figure of merit zT for the composite aerogel is modest when compared to the values of the composite films presented in Table 1. However, making comparisons is difficult due to the variation in electronic properties of poly(Ni-ett) from batch to batch. Regardless, this study proves that it is possible to reduce the thermal transport properties of an *n*-type material through the use of a fibrillar aerogel structure. Due to their macroscopic thickness (several millimetres), their low thermal conductivity and decent charge transport properties, these samples are suitable for use in thermoelectric applications. This makes them

particularly useful in vertical generators where a thermal gradient must be efficiently maintained [53].

4. Conclusion

In contrast to most research on polymer thermoelectrics that focuses on *p*-type and thin-film, we have demonstrated a 3D structuring approach for an *n*-type conducting polymer. This approach resulted in lightweight and robust aerogels (that can be manipulated with tweezers) with interesting thermoelectric properties. To achieve this, we first optimized the gelation conditions of the PVDF matrix used as scaffold before proposing a process to homogeneously disperse the poly(Ni-ett) within it. A mesoporous and fibrillar structure was obtained, for which thermal conductivity was reduced by five times compared to the dense pellet. The decrease in thermal conductivity compensated for the reduction in apparent electrical conductivity (caused by the high air content). The thermoelectric properties remained stable under an inert atmosphere and the charge transport properties of the composite aerogel showed only a slight decline upon air exposure. Further research is still needed to enhance the charge transport properties of the aerogels. In particular, an optimum between porosity and overall thermoelectric performance has yet to be found. However this study exemplifies an attractive novel approach for producing materials for lightweight and vertical thermoelectric generators. The process can also be easily adapted to other type of polymer blends or conducting fillers.

Acknowledgments:

ANR JCJC 2019 (BODYTEG: ANR-19- CE06-0004) and Région Grand Est 2020 are gratefully acknowledged for financial support. H.B. acknowledges financial support from the EPSRC (EP/W005875/1). B.C.S. acknowledges the UK Research and Innovation for Future Leaders Fellowship no. MR/S031952/1.

The CarMac platform of the ICS is acknowledged for GPC, TGA, DSC and IR characterizations. PLAMICS microscopy facility and DiffériX x-ray facility of the ICS are acknowledged for

technical support and the use of their equipment. Martin Brinkmann and C3-Fab platform (ICube) are acknowledged for providing access to the Seebeck measurement set-up and the collinear four-probe setup both located in a glove box, respectively. Nicolas Stein is thanked for the cross-plane Seebeck coefficient measurement. Ksenia Parkhomenko is acknowledged for the BET measurement. Patrick Allgayer, Christophe Lambour, Laurent Hermann and Jean-Philippe Lamps are thanked for technical support. Mohamed Oussama Bounab is thanked for his help on measuring thermal conductivity. Bhoje Gowd and Sruthi Suresh are thanked for valuable discussions on PVDF.

Supporting Information:

Schematic of the composite aerogel preparation; Digital images of the wet and dried composite gels; DSC of the composite aerogel; Nitrogen adsorption-desorption isotherms and BJH desorption pore volume plots for the PVDF:poly(Ni-ett) composite aerogel and the $PVDF_{N2L}$ aerogel; Physical and textural properties of the three samples; TGA curves; FTIR spectrum of the composite; schematic of the Seebeck coefficient measurement set-up and a typical curve

Conflict of interest:

There is no conflict to declare.

References

[1] B. Inc, Waste Heat Recovery: Technology Opportunities in the US Industry, Waste Heat Recover. Technol. Oppor. US Ind., 2008, 1–112. doi: 10.1017/CBO9781107415324.004.

[2] P. Fernández-Yáñez, V. Romero, O. Armas, and G. Cerretti, Thermal management of thermoelectric generators for waste energy recovery, Appl. Therm. Eng. 2021, 196, 117291. doi: 10.1016/j.applthermaleng.2021.117291.

[3] K. Zeb, S.M. Ali, B. Khan, C.A. Mehmood, N. Tareen, W. Din, U. Farid, A. Haider, A survey on waste heat recovery: Electric power generation and potential prospects within Pakistan, Renew. Sustain. Energy Rev. 2017, 75, 1142–1155. doi:

10.1016/j.rser.2016.11.096.

[4] J.-H. Bahk, H. Fang, K. Yazawa and A. Shakouri, Flexible thermoelectric materials and device optimization for wearable energy harvesting, J. Mater. Chem. C 2015, 3, 10362. https://doi.org/10.1039/C5TC01644D.

[5] H. Wang and C. Yu, Organic Thermoelectrics: Materials Preparation, Performance Optimization, and Device Integration, Joule 2019, 3, 53–80. doi: 10.1016/j.joule.2018.10.012.

[6] M. Massetti, F.Jiao, A. J. Ferguson, D. Zhao, K. Wijeratne, A. Würger, J. L. Blackburn, X. Crispin, and S. Fabiano, Unconventional Thermoelectric Materials for Energy Harvesting and Sensing Applications, Chem. Rev. 2021, 121, 20, 12465–12547. Doi: 10.1021/acs.chemrev.1c00218

[7] G. Prunet, F. Pawula, G. Fleury, E. Cloutet, A.J. Robinson, G. Hadziioannou, A. Pakde, A review on conductive polymers and their hybrids for flexible and wearable thermoelectric applications, Mater. Today Phys. 2021, 18, 100402. doi: 10.1016/j.mtphys.2021.100402.

[8] B. Meng, J. Liu, and L. Wang, Recent development of n-type thermoelectric materials based on conjugated polymers, Nano Mater. Sci., 2021, 3, 113–123. doi: 10.1016/j.nanoms.2020.10.002.

[9] R. Kroon, D. A. Mengistie, D.Kiefer, J. Hynynen, J. D. Ryan, L. Yua and C. Müller, Thermoelectric plastics: From design to synthesis, processing and structure-property relationships, Chem. Soc. Rev. 2016, 45, 6147–6164. doi: 10.1039/c6cs00149a.

[10] Y. Lu, J. Y. Wang, and J. Pei, Strategies to Enhance the Conductivity of n-Type Polymer Thermoelectric Materials, Chem. Mater. 2019, 31, 6412–6423. doi: 10.1021/acs.chemmater.9b01422.

[11] A. K. Menon, R. M. W. Wolfe, S. Kommandur, and S. K. Yee, Progress in Nickel-Coordinated Polymers as Intrinsically Conducting n-Type Thermoelectric Materials, Adv. Electron. Mater. 2019, 5, 1800884. doi: 10.1002/aelm.201800884.

[12] J. Tang, Y. Chen, S. R. McCuskey, L. Chen, G. C. Bazan, and Z. Liang, Recent Advances in n-Type Thermoelectric Nanocomposites, Adv. Electron. Mater. 2019, 5, 1800943. doi: 10.1002/aelm.201800943.

[13] Y. Lu and D. J. Young, Coordination polymers for n-type thermoelectric applications,

Dalt. Trans. 2020, 49, 7644–7657. doi: 10.1039/d0dt00872a.

[14] Z. Liu, M. A. Haque, C. N. Savory, T. Liu, S. Matsuishi, O. Fenwick, D.O. Scanlon, M. A. Zwijnenburg, D. Baran , B. C. Schroeder, Controlling the thermoelectric properties of organo-metallic coordination polymers through backbone geometry, Faraday Discuss. 2023, DOI: 10.1039/D3FD00139C.

[15] Y. Sun, P Sheng, C.Di, F. Jiao, W. Xu, D. Qiu, and D. Zhu, Organic thermoelectric materials and devices based on p- and n-type poly(metal 1,1,2,2-ethenetetrathiolate)s, Adv. Mater. 2012, 24, 932–937. doi: 10.1002/adma.201104305.

[16] F. Jiao, C.-A. Di, Y. Sun, P. Sheng, W. Xu, D. Zhu J., Inkjet-printed flexible organic thin-film thermoelectric devices based on p- and n-type poly(metal 1,1,2,2-ethenetetrathiolate)s / polymer composites through ball milling, Philos. Trans. R. Soc. A 2014, 372, 20130008. doi: 10.1098/rsta.2013.0008.

[17] A. K. Menon, E. Uzunlar, R. M. W. Wolfe, J. R. Reynolds, S. R. Marder, and S. K. Yee, Metallo-organic n-type thermoelectrics: Emphasizing advances in nickel-ethenetetrathiolates, J. Appl. Polym. Sci., 2017, 134, 44402. doi: 10.1002/app.44402.

[18] A. K. Menon, R. M. W. Wolfe, S. R. Marder, J. R. Reynolds, and S. K. Yee, Systematic Power Factor Enhancement in n-Type NiETT/PVDF Composite Films, Adv. Funct. Mater. 2018, 28, 1801620. doi: 10.1002/adfm.201801620.

[19] N. Toshima, K. Oshima, H. Anno, T. Nishinaka, S. Ichikawa, A. Iwata, Y. Shiraishi, Novel Hybrid Organic Thermoelectric Materials:Three-Component Hybrid Films Consisting of a Nanoparticle Polymer Complex, Carbon Nanotubes, and Vinyl Polymer, Adv. Mater. 2015, 27, 2246–2251. doi: 10.1002/adma.201405463.

[20] Q. Weinbach, C. B. Nielsen, and L. Biniek, Multi length scale porosity as a playground for organic thermoelectric applications, J. Mater. Chem. C 2021, 9, 10173–10192. doi: 10.1039/d1tc02331d.

[21] V. Apostolopoulou-Kalkavoura, P. Munier, and L. Bergström, Thermally Insulating Nanocellulose-Based Materials, Adv. Mater. 2021, 33, 2001839. doi: 10.1002/adma.202001839.

[22] M. Li, Z. Qin, Y. Cui, C. Yang, C. Deng, Y. Wang, J. S. Kang, H. Xia, Y. Hu, Ultralight and Flexible Monolithic Polymer Aerogel with Extraordinary Thermal Insulation by A Facile Ambient Process, Adv. Mater. Interfaces 2019, 6, 1900314. doi:

10.1002/admi.201900314.

[23] Kroon, R., Ryan, J. D., Kiefer, D., Yu, L., Hynynen, J., Olsson, E., and C. Müller, Bulk Doping of Millimeter-Thick Conjugated Polymer Foams for Plastic Thermoelectrics. Adv. Funct. Mater. 2017, 27, 1704183. doi:10.1002/adfm.201704183.

[24] X. Wang, P.Liu, Q. Jiang, W. Zhou, J. Xu, J. Liu, Y. Jia, X. Duan, Y. Liu, Y. Du, and F. Jiang, Efficient DMSO-Vapor Annealing for Enhancing Thermoelectric Performance of PEDOT:PSS-Based Aerogel, ACS Appl. Mater. Interfaces 2019, 11, 2408–2417. doi: 10.1021/acsami.8b19168.

[25] Q. Weinbach, S.V. Thakkar, A. Carvalho, G. Chaplais , J. Combet, D. Constantin, N. Stein, D. Collin and L. Biniek, Efficient Control of a Mesoporous Fibrillar PEDOT:PSS Aerogel Structure for Promising Thermoelectric Applications, Front. Electron. Mater. 2022, 2, 875856. doi: 10.3389/femat.2022.875856.

[26] M.P. Gordon, E.W. Zaia, P. Zhou, B. Russ, N.E. Coates, A. Sahu, J.J. Urban, Soft PEDOTSS aerogel architectures for thermoelectric applications, J. Appl. Polym. Sci. 2017, 134 44070. doi:10.1002/app.44070.

[27] S. Han, F. Jiao, Z.U. Khan, J. Edberg, S. Fabiano, X. Crispin, Thermoelectric polymer aerogels for pressure-temperature sensing applications, Adv. Funct. Mater. 2017, 27, 1703549. doi:10.1002/adfm.201703549.

[28] N. Okada, K. Sato, M. Yokoo, E. Kodama, S. Kanehashi, T. Shimomura, Thermoelectric Properties of Poly(3-hexylthiophene) Nanofiber Aerogels with a Giant Seebeck Coefficient, Acs Appl. Polym. Mater. 2021, 3, 455-463. doi:10.1021/acsapm.0c01185.

[29] N. T. Hung, A. R. T. Nugraha, and R. Saito, Thermoelectric properties of carbon nanotubes, Energies 2019, 12, 1–27. doi: 10.3390/en12234561.

[30] J. L. Blackburn, A. J. Ferguson, C. Cho, and J. C. Grunlan, Carbon-Nanotube-Based Thermoelectric Materials and Devices, Adv. Mater. 2018, 30, 1704386. doi: 10.1002/adma.201704386.

[31] M. Li, Q. Gong, P. Cao, H. Wang, J. Qiao, Y. Yu, W. Lu, J. Di, Z. Zhang, L. Zheng and Q. Li, Rational and wide-range tuning of CNT aerogel conductors with multifunctionalities, Nanoscale 2020, 12, 13771–13780. doi: 10.1039/d0nr03564e.

[32] K. Oshima, Y. Shiraishi, and N. Toshima, Novel nanodispersed polymer complex, poly(nickel 1,1,2,2-ethenetetrathiolate): Preparation and hybridization for n-type of

organic thermoelectric materials, Chem. Lett. 2015, 44, 1185–1187. doi: 10.1246/cl.150328.

[33] R. Tkachov, L. Stepien, R. Grafe, O. Guskova, A. Kiriy, F. Simon, H. Reith, K. Nielsch, G. Schierning, D. Kasinathan and C. Leyens, Polyethenetetrathiolate or polytetrathiooxalate? Improved synthesis, a comparative analysis of a prominent thermoelectric polymer and implications to the charge transport mechanism, Polym. Chem., 2018, 9, 4543–4555. doi: 10.1039/c8py00931g.

[34] Y. Sun, J. Zhang, L. Liu, Y. Qin, Y. Sun, W. Xu and D. Zhu., Optimization of the thermoelectric properties of poly(nickel-ethylenetetrathiolate) synthesized via potentiostatic deposition, Sci. China Chem. 2016, 59, 1323–1329. doi: 10.1007/s11426-016-0175-9.

[35] R. M. W. Wolfe, A. K. Menon, T. R. Fletcher, S. R. Marder, J. R. Reynolds, and S. K. Yee, Simultaneous Enhancement in Electrical Conductivity and Thermopower of n-Type NiETT/PVDF Composite Films by Annealing, Adv. Funct. Mater. 2018, 28, 1803275. doi: 10.1002/adfm.201803275.

[36] Zhang J., Kong Y., Shen X. Polyvinylidene fluoride aerogel with high thermal stability and low thermal conductivity, Materials letters 2020, 259, 126890. Doi: 10.1016/j.matlet.2019.126890.

[37] Z.Liu, T. Liu, C. N. Savory, J. P. Jurado, J. S. Reparaz, J. Li, L. Pan, C. F. J. Faul, I. P. Parkin, G. Sankar, S.Matsuishi, M. Campoy-Quiles, D. O. Scanlon, M. A. Zwijnenburg, O. Fenwick, B. C. Schroeder., Controlling the Thermoelectric Properties of Organometallic Coordination Polymers via Ligand Design, Adv. Funct. Mater. 2020, 30, 2003106. doi: 10.1002/adfm.202003106.

[38] X. Wang, L. Zhang, D. Sun, Q. An, H. Chen, Formation mechanism and crystallization of poly(vinylidene fluoride) membrane via immersion precipitation method. Desalination 2009, 236, 170-17. doi: 10.1016/j.desal.2007.10.064.

[39] C. Marega and A. Marigo. Influence of annealing and chain defects on the melting behaviour of poly(vinylidene fluoride), European Polymer Journal 2003, 39, 1713–1720. Doi: 10.1016/S0014-3057(03)00062-4.

[40] Q. Weinbach, N. Hmili, E. Gottis, G. Fleith, J. Combet, V. Papaefthimiou, V. Malesys, E. Denys, L. Simon, M. Schmutz, A. Carvalho, D. Constantin and L. Biniek, Tailoring the 3D

porous structure of conducting PEDOT:PSS gels via ice-templating, J. Mater. Chem. C 2023,11, 7802-7816. doi: 10.1039/D3TC01110K.

[41] Bohac, V., Gustavsson, M. K., Kubicar, L., and Gustafsson, S. E.. Parameter estimations for measurements of thermal transport properties with the hot disk thermal constants analyzer. Rev. Sci. Instrum. 2000, 71, 2452–2455. doi:10.1063/1.1150635.

[42] Topsøe, H. (1968). Geometric factors in four point resistivity measurement. Bridg. Technol. Bulletin n°472-13.

[43] A. Hamidi-Sakr, L.Biniek, J.-L. Bantignies, D. Maurin, L. Herrmann, N. Leclerc, P. Lévêque, V. Vijayakumar, N. Zimmermann, and M.Brinkmann, A Versatile Method to Fabricate Highly In-Plane Aligned Conducting Polymer Films with Anisotropic Charge Transport and Thermoelectric Properties, Adv. Funct. Mater. 2017, 1700173. doi: 10.1002/adfm.201700173.

[44] M. Pagliero, A. Bottino, A. Comite, and C. Costa, Novel hydrophobic PVDF membranes prepared by nonsolvent induced phase separation for membrane distillation, J. Memb. Sci., 2020, 596, 117575. doi: 10.1016/j.memsci.2019.117575.

[45] A. K. Hołda and I. F. J. Vankelecom, Understanding and guiding the phase inversion process for synthesis of solvent resistant nanofiltration membranes, J. Appl. Polym. Sci. 2015, 132, 1–17. doi: 10.1002/app.42130.

[46] X. Chen, Y. N. Liang, X. Tang, W. Shen, and X. Hu, Additive-free Poly (vinylidene fluoride) Aerogel for Oil / water Separation and Rapid Oil Absorption, Chem. Eng. J. 2016, 308, 18-26. doi: 10.1016/j.cej.2016.09.038.

[47] J.-M. Guenet, Polymer-Solvent Molecular Compounds. Elsevier Science, Amsterdam 2007.

[48] X. Cai, T. Lei, D. Sun and L. Lin, A critical analysis of the α, β and γ phases in poly(vinylidene fluoride) using FTIR, RSC Adv. 2017, 7, 15382-15389. doi: 10.1039/C7RA01267E.

[49] N. Meng, X. Ren, G. Santagiuliana, L. Ventura, H. Zhang, J. Wu, H. Yan, M.J. Reece, E. Bilotti, Ultrahigh β-phase content poly(vinylidene fluoride) with relaxor-like ferroelectricity for high energy density capacitors. Nat Commun. 2019, 10, 4535. doi:10.1038/s41467-019-12391-3.

[50] S. Suresh, T. Nabiyeva, L. Biniek, and E. B. Gowd, Poly(vinylidene fluoride) Aerogels with α, β, and γ Crystalline Forms: Correlating Physicochemical Properties with

Polymorphic Structures, ACS Polymers Au, 2024, accepted. doi: 10.1021/acspolymersau.3c00044

[51] R. M. Ireland, T. Jones, H. Li, H. Jang, J. E. West, and H. E. Katz, Statically Charged Electret Polymers as Solid, Nonvolatile Gates Encapsulating and Tuning Polymer Thermoelectric Parameters, ACS Energy Letters 2016, 1, 612. DOI: 10.1021/acsenergylett.6b00269

[52] K. Wan, P. J. Taroni, Z. Liu, Y. Liu, Y. Tu, G. Santagiuliana, I.C. Hsia, H. Zhang, O. Fenwick, S. Krause, M. Baxendale, B. C. Schroeder, E. Bilotti, Flexible and Stretchable Self-Powered Multi-Sensors Based on the N-Type Thermoelectric Response of Polyurethane/Na_x(Ni-ett)$_n$ Composites, Adv. Electron. Mater. 2019, 5, 1900582. doi: 10.1002/aelm.201900582

[53] X. Wang, L. Liang, H. Lv, Y. Zhang, and G. Chen, Elastic aerogel thermoelectric generator with vertical temperature-difference architecture and compression-induced power enhancement, Nano Energy 2021, 90, 106577. doi: 10.1016/j.nanoen.2021.106577.